Transactions, SMiRT-26
Berlin/Potsdam, Germany, July 10-15, 2022
Division IV

SIMULATION OF SURFACE FAULT DISPLACEMENT USING A MULTISCALE FINITE ELEMENT METHOD

Masataka Sawada[1], Kazumoto Haba[2], Kohei Fujita[3], Tsuyoshi Ichimura[4], Muneo Hori[5]

[1] Senior Research Scientist, Central Research Institute of Electric Power Industry, Abiko, Chiba, Japan (sawada@criepi.denken.or.jp)
[2] Manager, Taisei Corporation, Tokyo, Japan
[3] Associate Professor, The University of Tokyo, Tokyo, Japan
[4] Professor, The University of Tokyo, Tokyo, Japan
[5] Director-General, Japan Agency for Marine-Earth Science and Technology, Yokohama, Kanagawa, Japan

ABSTRACT

Continuum-mechanics-based numerical simulations are promising methods for evaluating surface fault displacements. We propose multiscale analysis using the parallel finite element method to evaluate both fault displacements and seismic ground motion. We applied the proposed numerical method to simulate the 2008 Iwate-Miyagi Nairiku earthquake, where surface faulting and strong ground motion were observed. We implemented a set of macro and micro models. We first obtained a solution for wide-area ground deformation history through macro analysis and then obtained a solution for surface fault displacement and seismic ground motion by incorporating the surface fault distribution and slip propagation into our micro analysis. The calculated surface slip occurrence was consistent with field observations of surface ruptures. The simulation results demonstrate that the occurrence of a surface earthquake fault causes larger surface ground motion in the vicinity of faults.

INTRODUCTION

Since the occurrence of massive earthquakes in Taiwan and Turkey in 1999, there has been growing concern regarding potential damage to various infrastructure systems and buildings caused by surface fault ruptures. For on-site fault assessment at nuclear power plants (NPPs), it is important to estimate fault displacements and their impact on facility safety functions. Following detailed geological surveys, important NPP facilities are separated from primary faults that are direct extensions of earthquake source faults. However, there may be secondary faults (sub-faults) located beneath or close to these important facilities. The effects of slip on such sub-faults have been discussed. Additionally, facilities affected by fault displacement are expected to be exposed to strong seismic motions simultaneously. Therefore, it is necessary to evaluate the effects of the superposition of fault displacement and earthquake ground motion.

Numerical simulations based on continuum mechanics are promising methods for estimating surface fault displacement. However, there are major difficulties in simulating fault rupture processes. One challenge is the requirement for significant numerical computations to simulate such processes for a target area that is only a few hundred meters in size. Another difficulty is stability loss in the solution of the initial and boundary value problems to which numerical analysis is applied. Stability implies that a solution does not change significantly when a small variation is added to the problem and stability loss leads to drastic changes in solutions induced by small disturbances in numerical computations.

We overcame these difficulties by applying high-performance computing (HPC) to solve a high-resolution analysis model (Sawada et al., 2017; Sawada et al., 2018a). We developed a finite element model (FEM) strengthened by the following two functions: (1) a symplectic time integration explicit scheme to conserve the energy of the system and (2) rigorously formulated high-order joint elements. These were implemented in the open-source parallel FEM program *FrontISTR*. Many other functions requested for earthquake engineering problems were also implemented in this program and are referred to as *E-FrontSITR* (Motoyama et al., 2021). Another use of HPC is to perform multicase analyses with different input conditions in parallel. This enabled us to evaluate the variability of generated solutions.

We applied the FEM to simulations of the 2014 Nagano-ken-hokubu earthquake and 2016 Kumamoto earthquake, where surface faults were observed (Sawada et al., 2018b; Sawada et al., 2022). We constructed analysis models with high fidelity for the $5 \times 5 \times 1$ km target domain, including primary and sub-faults. We adopted the following two-step simulation method: (1) evaluating the boundary displacement of the analysis model containing the target sub-faults by determining crustal deformation based on the elastic theory of dislocation (Okada, 1995) and (2) evaluating the spreading and dispersion of slip on the primary fault and sub-faults in our analysis models using the FEM. Through these simulations, we confirmed the applicability of the FEM to the evaluation of surface fault occurrence. We also estimated the effects of material uncertainty on surface fault displacement by performing 230 simulations using Latin hypercube sampling (Haba et al, 2020).

However, the elastic theory of dislocation is a static method and we have not been able to account for the effects of seismic motion deep underground in the simulations performed thus far. In this paper, we propose a multiscale FEM to evaluate the superposition of fault displacement and seismic motion.

NUMERICAL METHOD

Multiscale FEM

The stress-strain relationship of the ground, stress-slip relationship on the fault plane, and appropriate initial and boundary conditions are provided and a mathematical model of the continuum for fault behavior is established. In our previous simulations, we constructed analysis models of a $5 \times 5 \times 1$ km target domain and evaluated surface slip by calculating the spread and dispersion of the input slip at the bottom of the fault. However, in general, the source fault lengths of earthquakes in which surface earthquake faults appear exceed the size of this analytical model. Therefore, boundary conditions must be defined for wide-area analysis considering the entire earthquake source fault. In our previous simulations, the elasticity theory of dislocations was used for wide-area analysis.

To perform numerical analysis of the superposition of fault displacement and seismic ground motion, the analysis of a wide area must also be dynamic. Therefore, we decided to replace the elastic theory of dislocation with a dynamic FEM and conduct two-step dynamic FEM (multiscale FEM) earthquake motion simulations based on multiscale approaches, such as those reported by Bielak et al. (2003), Ichimura et al. (2007), Moczo et al. (1997), and Orsal and Zahradnik (2002). Figure 1 illustrates the target problem. To evaluate both surface fault displacement and seismic motion, we must solve a dynamic system from earthquake source faults to surface sub-faults. We decomposed the system into two subsystems with different scales. We performed dynamic analysis of an earthquake source fault on the surface without sub-faults or structures (macro analysis). Next, we analyzed a small region containing sub-faults and structures.

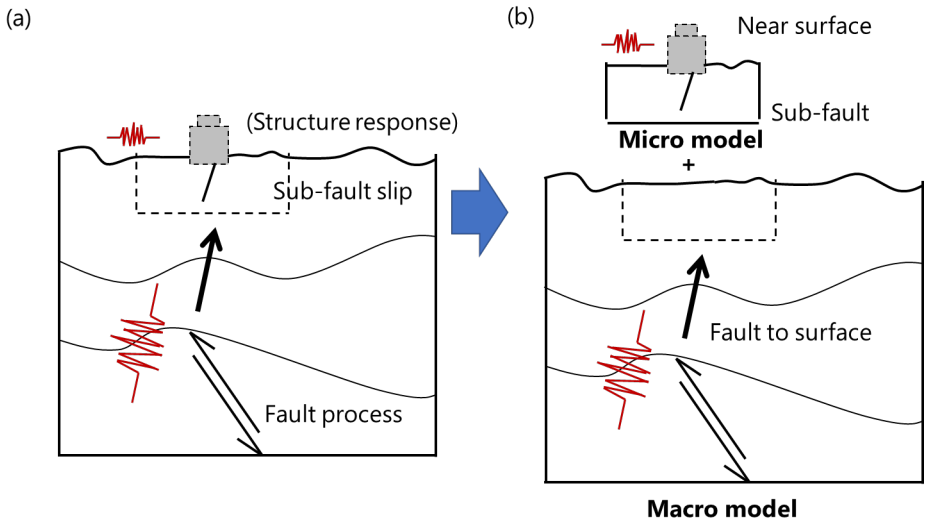

Figure 1. Schematic view of the target problem: (a) system from the earthquake source fault to surface sub-faults and (b) decomposed system in the multiscale FEM. We performed analysis from the earthquake source fault to a surface without sub-faults and structures (macro analysis). We then analyzed the small region containing the sub-faults and structures (micro analysis).

Constitutive model of faults

We implemented joint elements using a nonlinear spring-type constitutive equation to represent fault movement. The constitutive equation for the shear movement of the joint elements is defined as follows (Fig. 2):

$$\tau = \kappa u, \tag{1}$$

where τ is the shear stress and u is the slip on the fault plane. The spring coefficient per unit area (shear stiffness) κ is described by the following function for slip u:

$$\kappa(u) = \begin{cases} \kappa_0 - \frac{\kappa_0 - \kappa_d}{u_{cr}} u & (u \le u_{cr}) \\ \kappa_d & (u > u_{cr}) \end{cases}, \tag{2}$$

where κ_0 denotes the initial shear stiffness, κ_d denotes the final shear stiffness, and u_{cr} denotes the critical slip. We considered the effects of the normal stress on the shear stiffness of the faults and defined the following equation:

$$\kappa_0 = \tilde{\kappa}_0(\sigma_n + b), \tag{3}$$

where $\tilde{\kappa}_0$ is the shear stiffness per unit of normal stress, σ_n is the normal stress on the fault plane; and b is a constant. We assume that the first peak of the slip-shear stress relationship presented in Fig. 2 is identical to the shear strength. The parameters $\tilde{\kappa}_0$ and b in Equation (3) can be determined such that the shear strength satisfies Coulomb's law of friction as follows:

$$\tilde{\kappa}_0 = \frac{4(1-\kappa_d/\kappa_0)}{u_{cr}} \tan\phi, \tag{4}$$

$$b = \frac{4c}{\tilde{\kappa}_0 u_{cr}} (1 - \kappa_d/\kappa_0), \tag{5}$$

where c is the cohesion and ϕ is the friction angle.

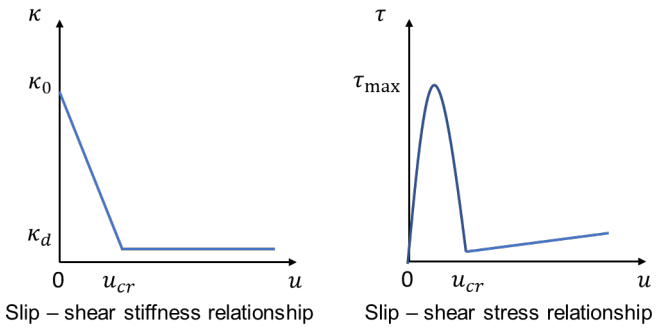

Figure 2. Nonlinear slip-shear stress relationship.

When conducting dynamic analysis, we assumed that when the direction of the fault slip reverses, the shear stiffness recovers to its initial value. When the direction of the slip velocity changes by 90° or more relative to the previous step, the slip is judged to have reversed. Figure 3 presents the typical slip-shear stress relationship in cases where the slip direction reverses.

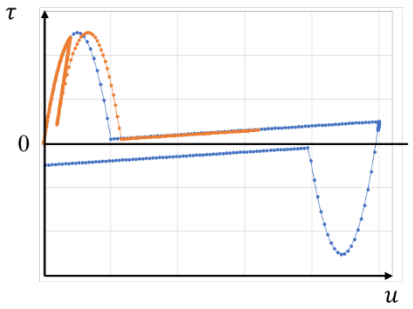

Figure 3. Typical slip-shear stress relationship in cases of slip direction reversal. The blue plot shows the relationship in the case where the slip direction reverses after slip weakening and the orange plot shows the relationship in the case where the slip direction reverses before the shear stress reaches the peak strength and reverses again.

SIMULATIONS

The 2008 Iwate-Miyagi Nairiku earthquake

The 2008 Iwate-Miyagi Nairiki earthquake was selected as the target earthquake for our test simulations. The earthquake was an M_{JMA} 7.2 (Japan Meteorological Agency [JMA]) reverse-fault-type crustal earthquake that occurred on the eastern side of the Ou mountain range, northeast Honshu Island, Japan at 8:43 on June 14, 2008, Japanese standard time (23:43 on June 13, coordinated universal time). In this earthquake, the largest ground acceleration to date of 4022 cm/s^2 (vector sum of three components) was recorded at the hanging-wall station IWTH25 (West Ichinoseki) of the KiK-net, which is a strong-motion network operated by the National Research Institute for Earth Science and Disaster Prevention (NIED). KiK-net stations are equipped with seismometers not only on the ground surface, but also in boreholes. The borehole accelerator at IWTH25, which is installed 260 m below ground level in soft rock, also recorded an acceleration exceeding 1000 cm/s^2. Additionally, surface fault ruptures were observed intermittently along the eastern margin of the aftershock zone. The total length of the tectonic breakage zone was approximately 20 km (Toda et al., 2010).

Asano and Iwata (2011) conducted seismic source inversion analysis of the 2008 Iwate-Miyagi Nairiku earthquake and obtained the slip distributions on the earthquake source fault, as shown in Fig. 4. In their analysis, the length of the fault was 38 km and the depth of the upper edge of the fault was 776 m.

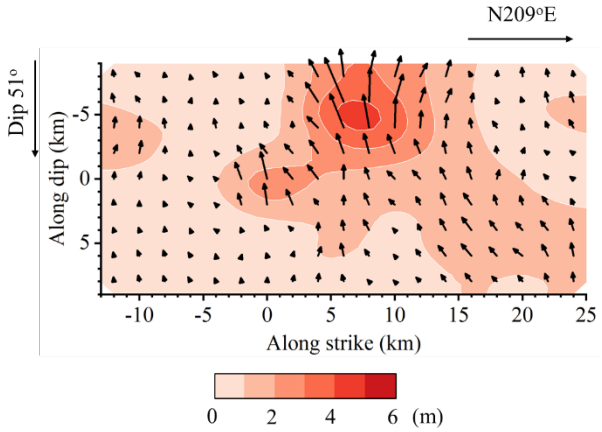

Figure 4. Slip distribution on the earthquake source fault.

Analysis model

Figure 5 presents the target of our macro analysis. The macro model covers a 40 × 50 km area from the surface to EL. −28 km, including the entire 38-km-long source fault. The upper edge of the fault was set to EL. −776 m. The micro model covers a 15 × 10 km area from the surface to EL. −776 m. The location of the micro model within the macro model is illustrated in Fig. 5. NIED provides a database of crustal structure densities and elastic wave velocities covering all of Japan through the Japan Seismic Hazard Information Station (J-SHIS) database. In this database, elevation data for the ground surface and boundaries of elastic wave velocity and density are provided at the center of every grid with a resolution of 30 arcseconds for latitude and 45 arcseconds for longitude. Using this database, we constructed analytical models that included the shape of the land and crustal structure. We determined the strike and dip angles, as well as the size of the earthquake source fault, using data reported by Asano and Iwata (2011).

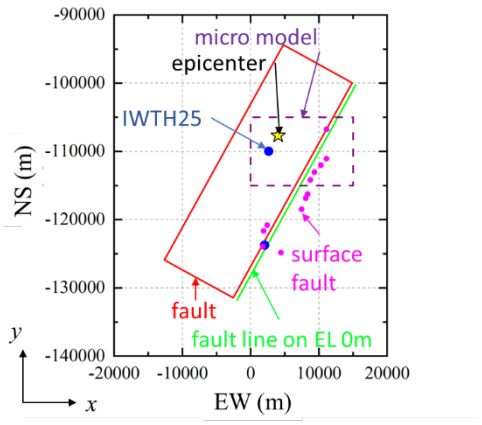

Figure 5. Target area for macro analysis. The red-lined square represents the earthquake source fault identified by Asano and Iwata (2011). The green line is the fault line of the extension from the earthquake source fault at EL. 0 m. The purple-dashed square represents the target area of micro analysis. Pink plots represent observed surface ruptures described by Toda et al. (2010).

Figure 6 presents the macro and micro analysis models. For the first test simulation of the multiscale FEM, we only included the extension of the seismic source fault and did not include any sub-faults or structures. The ground was divided into second-order tetrahedral solid elements. In the macro model, a finite-element mesh was created without considering the presence of faults. In contrast, in the micro model, the fault was extended to the ground surface at the same dip angle and represented by second-order triangle joint elements.

The macro model was divided into eight layers with different material properties. The micro model included four of the eight layers. Table 1 lists the material properties of each layer. The ground was assumed to be a linear elastic body and the Young's modulus and Poisson's ratio of each layer were derived from the density and elastic wave velocity values in the J-SHIS database. The database also provides Q values related to damping. The damping ratio h is derived from the Q value using the following equation:

$$h = \frac{1}{2Q}. \tag{6}$$

We determined the coefficients of Rayleigh damping such that the damping ratio did not exceed h at frequencies from 0.1 to 4 Hz.

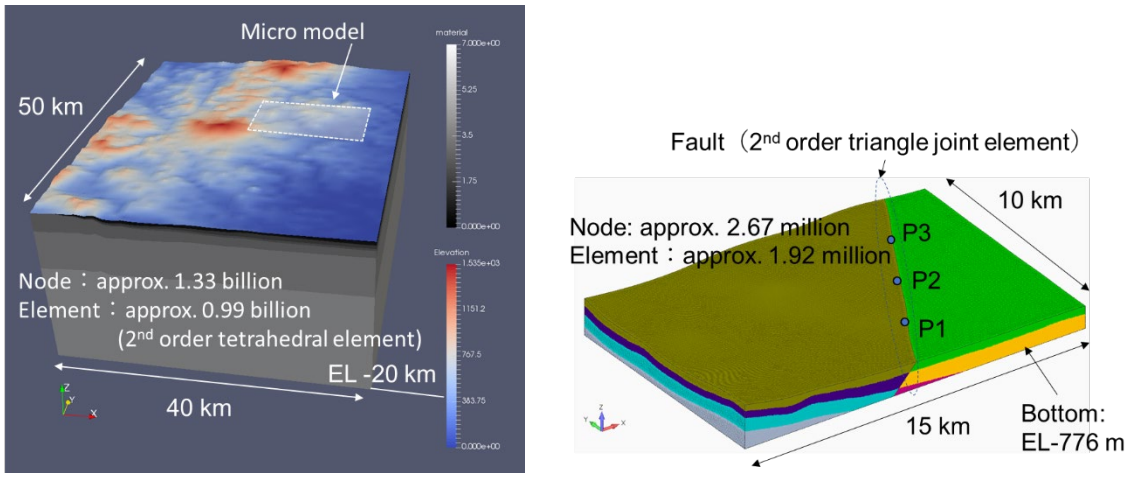

(a) Macro model (b) Micro model

Figure 6. Analysis models. (a) Macro model: The grayscale contour represents crustal structure and the blue-to-red contour represents ground surface altitude. (b) Micro model: The model is divided into four layers with different material properties. The layers are further divided by the fault. The analysis model is displayed with color-coded blocks divided by fault and property boundaries.

Table 1. Material properties of the ground

Layer	P-wave velocity (m/s)	S-wave velocity (m/s)	Density (kg/m^3)	Q value
1*	2000	600	1900	100
2	2500	1100	2150	150
3*	3000	1400	2250	150
4	3500	1700	2300	150
5	4000	2100	2400	200
6	5500	3100	2600	300
7*	5700	3300	2700	300
8*	6000	3400	2750	300

* These layers do not exist or are too thin to be included in the micro model.

Table 2. Material parameters for the fault.

Friction angle (deg)	Cohesion (MPa)	Shear stiffness ratio κ_d/κ_0	Critical slip (m)
25	0.025	0.01	0.1

We assumed a cohesion of 0.025 MPa and friction angle of 25° on the fault plane based on the experimental values of the crushed zones at NPP sites. The ratio between the initial and final shear stiffness κ_d/κ_0 was assumed to be 0.01 based on analyses conducted using a simple ground/fault model and real earthquake ground model (Sawada et al., 2018a, 2018b). The critical slip u_{cr} was 0.1 m based on the value used in the dynamic rupture simulation of the fault (Kase and Kuge, 2001). The material parameter values for the fault are summarized in Table 2.

In the macro analysis, we defined double-couple point sources at the nodes around the fault based on the seismic moment distribution calculated from the slip distribution presented in Fig. 4. Although it is necessary to simulate slip propagation from the rupture initiation point, in the following simulation, it was assumed that the entire fault slipped simultaneously according to the function presented in Fig. 7. The analysis was conducted for 20 s from the start of fault rupture with a time increment of 0.01 s (2000 steps). An absorbing boundary condition based on the study by Lysmer and Kuhlemeyer (1962) was applied to the bottom and four sides of the model. The macro model was large with more than 1.3 billion nodes and parallel computation was performed using 8192 CPU cores (512 MPI processes × 16 threads) based on an FEM program developed for supercomputers by Ichimura et al. (2014). The simulation took approximately 2.5 h. The nodal force and nodal velocity histories at the boundaries of the micro model were also computed.

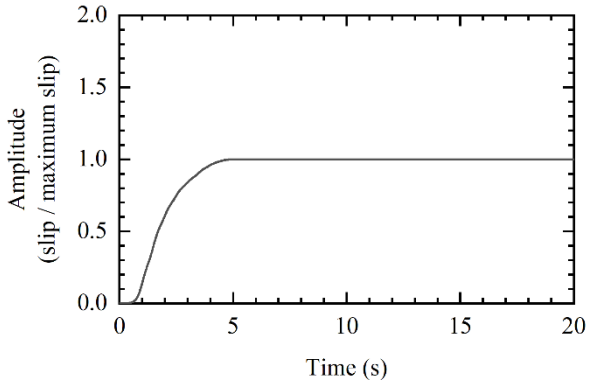

Figure 7. Slip function. The entire fault slips simultaneously according to this function. The slip magnitude and rake angle follow Fig. 5.

We conducted initial stress analysis to determine the values of parameters $\tilde{\kappa}_0$ and b on the fault plane using Equations (4) and (5) prior to our micro analyses. Normal displacements were fixed at the bottom and side boundaries during the initial stress analyses. For micro analysis, we defined absorbing and infinite boundary conditions and applied the nodal force and nodal velocity histories to the boundaries. We also applied slip to the bottom of the fault. We conducted micro analysis through parallel computation on 120 CPU cores using *E-FrontISTR*.

Results

Figure 8 presents the contours of the final surface displacement obtained from macro analysis. The near-surface slip at the center of the fault is large, as shown in Fig. 4, and the surface displacements are consistent with this phenomenon. In the micro model area, the displacement is larger on the southern side.

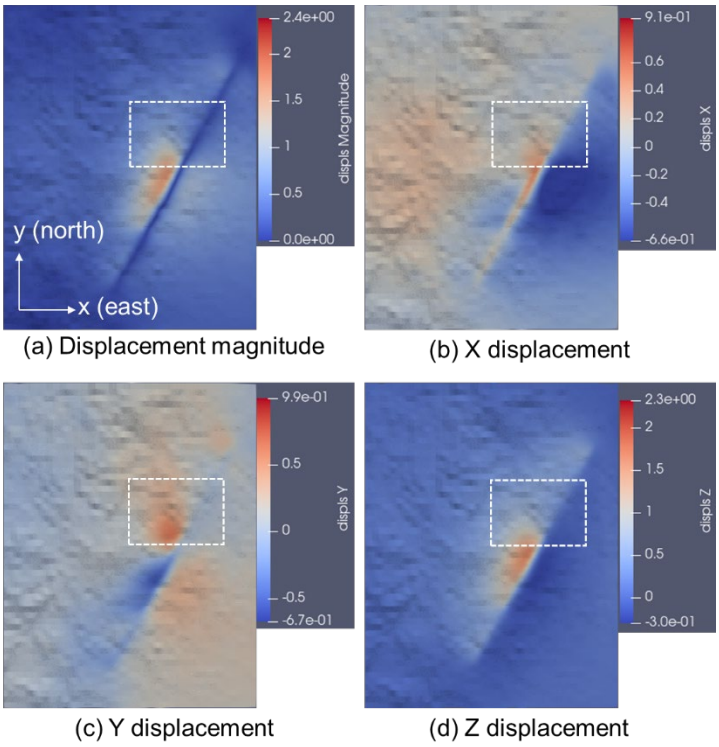

Figure 8. Contours of surface displacement after 20 s obtained from macro analysis. The white-dashed square shows the area of the micro model. The unit of displacement is meters.

Figure 9 presents the slip propagation on the fault obtained through micro analysis. The slip propagates from the bottom to the southern section of the surface between the southern edge and P1. Slip propagation is almost complete within three seconds. The input slip is large in the surface-ruptured section. As shown in Fig. 5, surface ruptures were observed in the middle of the upper edge of the fault (i.e., the southern part of the micro model), which is consistent with the results of numerical simulations.

Figure 10 presents the maximum surface velocity distribution. In this figure, we compare the results of simulations with and without fault slip in the micro model. In the case of fault slip, areas of increased surface velocity can be observed in the vicinity of the fault. This tendency is especially obvious in the area where surface displacement occurs. However, the maximum surface velocity at large distances from the surface fault exhibits little difference depending on whether the fault ruptures in the micro model.

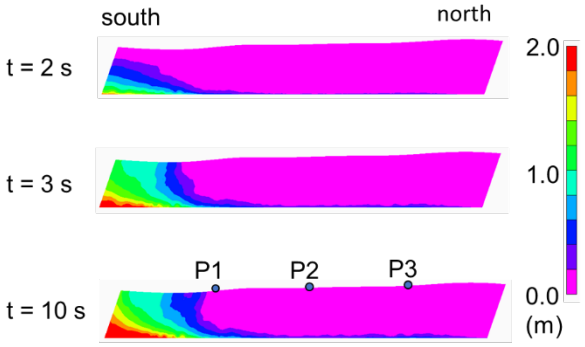

Figure 9. Slip propagation on the fault. P1, P2, and P3 divide the fault into four sections of equal length.

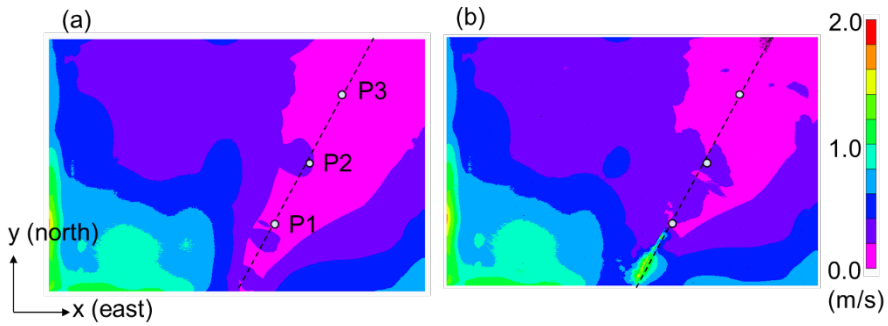

Figure 10. Contours of maximum surface velocity (x component). (a) Results from the simulation without fault slip. (b) Results from the simulation with fault slip.

Discussion

We conducted dynamic multiscale FEM analysis of fault ruptures. In our macro analysis, fault ruptures were represented by a kinematic source model. For micro analysis, the fault rupture propagated according to the mechanical constitutive law on the fault plane while the nodal forces obtained from macro analysis acted as boundary conditions. In our simulations, surface faulting consistent with field observations was obtained. For surface seismic motions, the numerical results indicated that the seismic motions caused the occurrence of surface faults in the micro analysis were additive with those caused by seismic sources deep underground in the macro analysis.

To compare and validate the calculated surface earthquake ground motions relative to observed records, it is necessary to establish a robust source process for the evolution of slip from the rupture initiation point. In this study, the fault constitutive law used for static analysis was modified and used for dynamic analysis. However, further study is required on a constitutive law suitable for the dynamic rupture analysis of surface faults.

CONCLUSIONS

In this paper, we proposed a multiscale analysis method using a parallel FEM to evaluate both fault displacements and seismic ground motion. We applied a numerical method to simulate the 2008 Iwate-Miyagi Nairiku earthquake, where surface faulting and strong ground motion were observed. We constructed a set of macro and micro models. We first obtained a solution for the wide-area ground deformation history through macro analysis and then obtained a solution for surface fault displacement and seismic ground motion by including the surface fault distribution and slip propagation results in micro analysis. The calculated surface slip occurrence was consistent with field-observed surface ruptures. Simulation results indicated that the occurrence of a surface earthquake fault causes larger surface earthquake ground motion in the vicinity of faults. These results demonstrate the applicability of the proposed method to the evaluation of the superposition effect of fault displacement and seismic ground vibration on important facilities.

REFERENCES

Asano, K. and Iwata, T. (2011). “Characterization of stress drops on asperities estimated from the heterogeneous kinematic slip model for strong motion prediction for inland crustal earthquakes in Japan,” *Pure Appl. Geophys.*, 168 105–116.

Bielak, J. Loukakis, K., Hisada, Y., and Yoshimura, C. (2003). “Domain reduction method for three-dimensional earthquake modelling in localized regions, Part I: Theory,” *Bull. Seismol. Soc. Am.*, 93(2) 817–824.

Ichimura, T., Hori, M., and Kuwamoto, H. (2007). "Earthquake motion simulation with multiscale finite-element analysis on hybrid grid," *Bull. Seismol. Soc. Am.*, 97(4) 1133–1143.

Ichimura, T., Fujita, K., Tanaka, S., Hori, M., Lalith, M., Shizawa, Y., and Kobayashi, H. (2014). "Physics-based urban earthquake simulation enhanced by 10.7 BlnDOE x 30 K time-step unstructured FE non-linear seismic wave simulation," *SC14*, 15–26.

FrontISTR. Available online: https://www.frontistr.com (accessed on 7 December 2021).

Haba, K., Hata, A., Sawada, M., and Hori, M. (2020). "Estimation of the effect of material uncertainty on surface fault displacement using Latin hyper cube sampling," *J. Jpn. Assoc. Earthq. Eng.*, 20 13–25. (In Japanese)

Japan Seismic Hazard Information Station. Available online: http://www.j-shis.bosai.go.jp (accessed on 7 December 2021).

Kase, Y. and Kuge, K. (2001). "Rupture propagation beyond fault discontinuities: significance of fault strike and location," *Geophys. J. Int.*, 147 330–342.

Lysmer, J. and Kuhlemeyer, R. L. (1969). "Finite dynamic model for infinite media," *Journal of Engineering Mechanics Division*, 95 859–878.

Moczo, P. Bystrický, E., Carcione, J. M., and Bouchon, M. (1997). "Hybrid modelling of P-SV seismic motion at inhomogeneous viscoelastic topographic structures," *Bull. Seismol. Soc. Am.*, 87(5) 1305–1323.

Motoyama, H., Sawada, M., Hotta, W., Haba, K., Otsuka, Y., Akiba, H., and Hori, M. (2021). "Development of a general-purpose parallel finite element method for analyzing earthquake engineering problems," *Earthquake Engng. Struct. Dyn.*, 50 4180–4198.

Okada, Y. (1992). "Internal deformation due to shear and tensile faults in a half-space," *Bull. Seismol. Soc. Am.*, 82 1018–1040.

Oprsal, I. and Zahradnik, J. (2002). "Three-dimensional finite difference method and hybrid modelling of earthquake ground motion," *J Geophys. Resear.*, 107 B8 2161, 10.1029/2000JB000082.

Sawada, M., Haba, K., and Hori, M. (2017). "High performance computing for fault displacement simulation," *J. JSCE*, 73 I_699-I_710. (In Japanese)

Sawada, M., Haba, K., and Hori, M. (2018a). "Estimation of surface fault displacement by high performance computing," *J. Earthq. Tsunami*, 12 181003.

Sawada, M., Haba, K., and Hori, M. (2018b). "Evaluation of surface fault displacement in a real earthquake with surface faulting by high performance computing," *J. JSCE*, 74 I_627-I_638. (In Japanese)

Sawada, M., Haba, K., and Hori, M. (2022). "Predictive simulation for surface fault occurrence using high-performance computing," *Geohazards*, 3 88–105.

Toda, S., Maruyama, T., Yoshimi, M., Kaneda, H., Awata, Y., Yoshioka, T., and Ando, R. (2010). "Surface rupture associated with the 2008 Iwate-Miyagi Nairiku, Japan, earthquake and its implications to the rupture process and evaluation of active faults," *J. Seism. Soc. Jpn., 2nd ser. Zisin*, 62 153–178. (In Japanese)